A geochemical application of the ITRAX scanner to a sediment core containing eastern Mediterranean sapropel units

J. THOMSON, I. W. CROUDACE & R. G. ROTHWELL
National Oceanography Centre, Empress Dock, Southampton SO14 3ZH, UK

Abstract: The ITRAX micro-X-ray fluoresence (XRF) core scanner has been applied in a sediment geochemistry investigation. The core sections selected contain examples of the organic-rich sedimentary units (sapropels) that form periodically in the eastern Mediterranean basin. Sapropels are visually obvious from their dark coloration, but the ITRAX X-radiograph also reveals physical property changes that result mainly from the high pore-water content of sapropels. A consideration of wavelength-dispersive XRF data from discrete samples of the most recent sapropel (S1) was made along with the set of elements reported by the ITRAX instrument's energy-dispersive XRF system over core sections containing S1. This allowed selection of a suite of eight inter-element ratios or element integrals through which characteristic features of sapropel development and geochemistry were revealed. While recognizing that the measured XRF element integrals from the ITRAX do not have an exact constant relationship with element concentration over changing sediment types, this combination of ratios provides significant information for geochemical interpretation. These include evidence for: (i) the presence of high C_{org} contents in the visual sapropel from Ba/Ti and Br/Cl ratios; (ii) a thinning of the original sapropel thickness by post-depositional oxidation from Mn/Ti and Cu/Ti ratios; (iii) pyrite authigenesis in the residual visual sapropel from Fe/Ti and S/Cl ratios and the As integral; and (iv) aragonite formation in and around the sapropel from the Sr/Ca ratio. These same ratios were then used to interpret ITRAX data from a deeper section of the same core containing the older sapropel S3, where the same characteristics, including the relict post-depositional oxidative thinning of the original unit, could be identified with only minor differences of detail. Directions of supply of Fe, As and Cu into the sapropels could be inferred from profile shapes.

The often-continuous record of past environmental conditions and changes that is contained in deep-sea sediments makes them a valuable resource for palaeoceanographic and palaeoclimatological research. Detailed sampling for specialist investigations at marine core repositories is greatly facilitated if logging data are available that profile some aspect of the changes in sediment characteristics that occur downcore. Current logging techniques include gamma-ray attenuation, P-wave attenuation and X-radiography that give information on changes in sediment density, and digital photography, magnetic susceptibility and X-ray fluorescence that give information on changes in sediment composition. The ITRAX instrument, developed by Cox Analytical Systems of Gothenburg in association with Southampton Oceanography Centre (SOC, renamed as National Oceanography Centre, Southampton – NOCS – 1 May 2005), is a new micro-X-ray fluorescence (XRF) and micro-X-radiograph scanner designed for rapid, automatic, non-destructive characterization of the optical, density and chemical composition variations in split sediment cores (Croudace *et al.* 2006).

Compositional data from energy-dispersive XRF (ED-XRF) scanners, for example the CORTEX system (Jansen *et al.* 1998), have mainly been applied to:

- studies of climatologically driven cyclicities in sediment deposition that are reflected, for instance, in $CaCO_3$ or Fe content fluctuations over time (e.g. Peterson *et al.* 2000; Palike *et al.* 2001); or
- sedimentological applications, where features such as ash layers, turbidite units or ice-rafted deposits may be recognized through their exotic compositions or their localized or organized bed characteristics (e.g. Hebbeln & Cortes 2001; Richter *et al.* 2001; Rothwell *et al.* 2006).

A further obvious application is to diagenetic geochemical studies, where the key is identification of unusually high contents of redox-sensitive elements in arrangements that are characteristic of some diagenetic process. Initial experience with the ITRAX system at the British Ocean Sediment Core Research Facility (BOSCORF) at SOC in such a diagenetic application is presented here. A wealth of published geochemical

From: ROTHWELL, R.G. 2006. *New Techniques in Sediment Core Analysis*. Geological Society, London, Special Publications, **267**, 65–77. 0305-8719/06/$15.00

information and interpretation is now available on eastern Mediterranean sapropels, particularly on the most recent interval, sapropel S1. An example of this unit was first examined to ascertain which elements measured by the ITRAX core scanner yield information on the characteristic elemental distributions that are known to occur in S1 from data measured on discrete samples by conventional techniques. Profile scans of the same elements from the next oldest sapropel (S3) that occurs deeper in the same core were then examined in the light of this experience with the S1 profile scans.

Material and methods

Core LC21 is a 10 cm-diameter giant (Calypso) piston core collected from a topographic high to the west of Karpathos Basin, NE of Crete, at 35°39.71′N, 26°34.96′E in 1522 m water depth (Rothwell 1995). The core is 13.5 m long and is stored at BOSCORF as 11 sections of 1.5 or 1.0 m nominal length. Sapropel S1 in particular from this core has been comprehensively investigated (Mercone *et al.* 2000, 2001; Casford *et al.* 2001, 2003; Rohling *et al.* 2002), and can be considered as a reference core for the Aegean area of the eastern Mediterranean during S1 times.

Core SL104 is a 4.8 m-long, 11 cm-diameter gravity core collected SE of Crete on *Meteor* cruise M51-3 at 34°48.89′N, 27°16.96′E in 2155 m water depth (Hemleben *et al.* 2001). The subsections of the core examined in this work were contained in polyvinyl chloride (PVC) U-channels of 1 m length by 2 × 2 cm cross-section that are often used in logging magnetic parameters (Weeks *et al.* 1993).

A more detailed description of the prototype ITRAX core scanner used is presented elsewhere (Croudace *et al.* 2006), and only an outline description is presented here. The instrument is computer controlled and designed for automatic, high-resolution logging of sections of split-sediment cores up to 10 cm in diameter and 1.8 m in length. Core sections are first scanned to ascertain whether a constant working distance for the X-ray detector can be achieved, using a laser distance finder to map the topography of the cut core surface. Regions where the detector will be retracted to avoid contact with the core surface are recorded. Simultaneously, a digital line camera captures a photographic image of the whole core surface. This process requires approximately 2 min for a core section 1 m long.

After photography, the core is automatically returned to the zero position and a stepper motor drives the scan at a line resolution that can be as fine as 100 μm. At each measurement position a 2 cm-wide high-resolution X-radiograph is recorded using a charge-coupled device (CCD) line camera and an ED-XRF spectrum is recorded using a Si-drift chamber detector. The time for each measurement, selected by the operator and dependent on the element detection sensitivity required, is typically 600–700 ms and 10–40 s, respectively. The X-ray beam used to irradiate the core section is generated from a 3 kW Mo target (typically run at 55 kV and 50 mA) that is focused through a flat capillary waveguide. Each ED-XRF spectrum recorded is stored along with header data, but spectra are also deconvolved in live time to build up profiles of peak area integrals for individual elemental and the coherent (Rayleigh) and incoherent (Compton) X-ray scattering peaks. These elemental peak areas are roughly proportional to the concentrations of major and trace elements present in the sediment. For the core LC21 and SL104 sections, scans were made every 0.5 mm with an excitation slit dimension of 20 mm × 200 μm and XRF analysis times of 35 or 45 s per measurement, so that processing each 1 m of core required 20–25 h.

Results and discussion

Inorganic geochemistry of sapropels

The sediments deposited in the eastern Mediterranean basin are mostly C_{org} and sulphide-poor clayey nannofossil oozes (subsequently referred to as 'marls'), but sapropels, sharply-defined dark sedimentary units with high contents of organic matter (C_{org}) and sulphide, occur as discrete beds within the sequence (Calvert 1983; Wehausen & Brumsack 2000; Calvert & Fontugne 2001). Sapropels form only at times of maximum summer insolation in the northern hemisphere, with a frequency of 23 ka mainly set by variations in the Earth's orbital precession (Rossignol-Strick 1983; Hilgen 1991; Lourens *et al.* 1996; Tuenter *et al.* 2003). Each sapropel has a duration of only a few thousand years, and not every insolation maximum produces a sapropel (van Santvoort *et al.* 1997; Bard *et al.* 2002). Inorganic geochemical investigations of the compositional differences between the enclosing marls and sapropels have demonstrated that many redox-sensitive elements show large systematic enrichments in sapropels (e.g. Calvert 1983; Thomson *et al.* 1995; Nijenhuis *et al.* 1999; Wehausen & Brumsack 2000; Calvert & Fontugne 2001; Mercone *et al.* 2001).

Sapropel S1 formed between 10 and 6 ^{14}C ka BP (Mercone *et al.* 2000). Mercone *et al.* (2001) investigated its inorganic geochemistry in core LC21 with wavelength-dispersive XRF (WD-XRF) data and coulometric C_{org} and $CaCO_3$ analysis (Figs 1 & 2). As in most sapropels, the $CaCO_3$ content of sapropel S1 is lower than

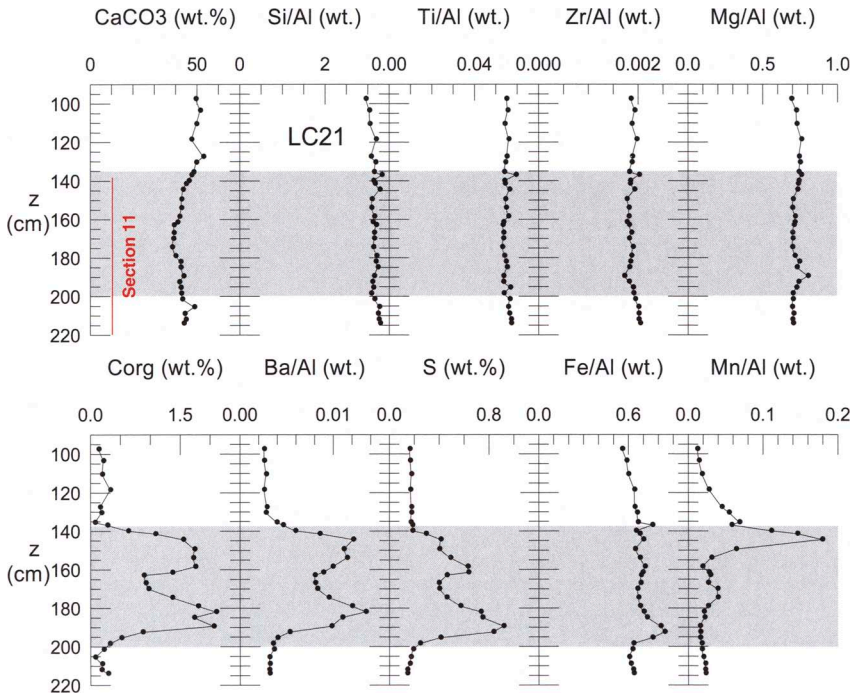

Fig. 1. $CaCO_3$, C_{org} and S concentration (wt%) and Al-normalized mass ratios of Si, Ti, Zr, Mg, Ba, Fe and Mn v. depth in core LC21 (after Mercone *et al.* 2001). All data are from WD-XRF except C_{org} and $CaCO_3$ which were measured by coulometry. The depth axis is cm below sea floor, and section 11 of the core containing sapropel S1 is at 138.5–219.5 cm below sea floor. The lightly shaded zone indicates sapropel S1.

those of the marls that enclose it, and, because biogenic $CaCO_3$ is a relatively pure phase, the concentrations of elements mainly present in the detrital aluminosilicate phase (e.g. Si, Al, Ti, K, Rb, Zr) must increase in the sapropel as a direct consequence of the decrease in $CaCO_3$ content. Geochemical data are therefore often expressed as a ratio to Al or some other element that is taken to be characteristic of the detrital phase in order to overcome this closed sum effect (Rollinson 1993; van der Weijden 2002).

In contrast to the essentially constant element/Al ratios found for the detrital elements (Fig. 1), many redox-sensitive elements when normalized to Al show distinct enrichments within sapropel S1 compared with the lower (detrital) levels observed in the enclosing marls (Figs 1 and 2). The S1 sapropel in core LC21 has two distinct lobes, although the central region still has a much higher C_{org} content than the marls above and below. Besides C_{org}, the elements showing the clearest enrichments in these two lobes are the C_{org} or sulphide-associated elements S, Fe, As, Mo and V. Other chalcophile elements (e.g. Cu, Ni, Pb and Zn) also show enrichments in the lobes of the sapropel, although the magnitude of these enrichments in excess of the detrital element/Al ratio is less marked than for As, V and Mo. In the enclosing marls, the concentrations of As and Mo are close to or below the detection limit of the WD-XRF instrument used, but both elements are readily detectable within the sapropel.

The relationship between the concentration of an element in the sediment (as measured for example by WD-XRF) and its peak area integral measured by ED-XRF excitation will not necessarily be constant along a core section of wet sediment (Jansen *et al.* 1998). Fluctuations in sediment mineralogy, particle size or water content, for example, will all influence the mean atomic number of the sediment under the X-ray excitation beam and, hence, affect the X-ray absorption and Compton and Rayleigh scattering. Thus, the higher water content of sapropels causes an increase in Compton scattering compared with the enclosing marls, and this alters the sensitivity of the system for different elements by different amounts. While recognizing the problems presented by such fluctuations in detection efficiency, a selection of parameters was made based on a consideration of: (i) the data of

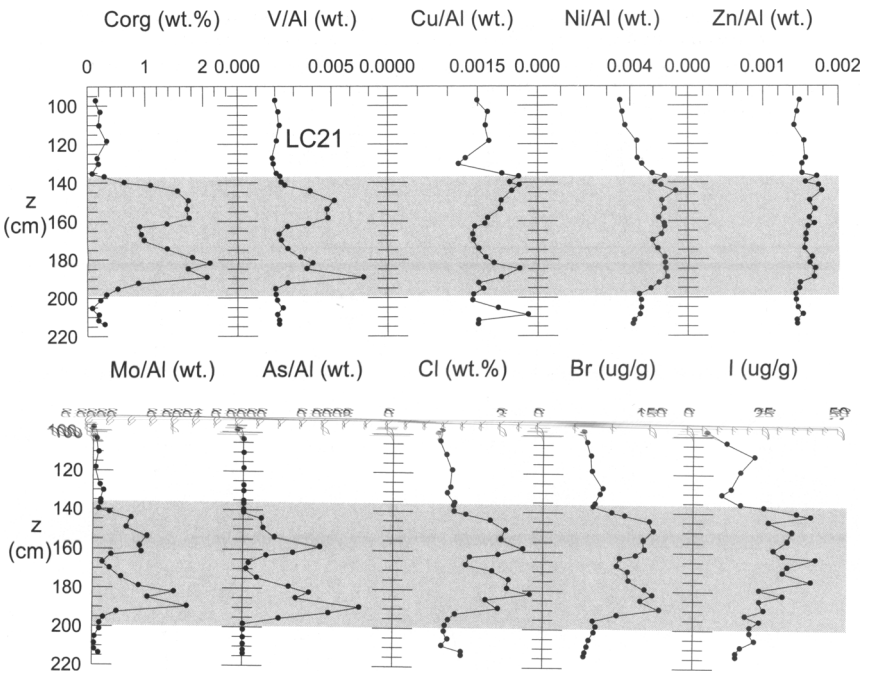

Fig. 2. C_{org} and Cl (wt%), Br and I ($\mu g\,g^{-1}$), Al-normalized mass ratios V, Cu, Ni, Zn, Mo, As v. depth in core LC21. All data except C_{org} are from WD-XRF. The depth axis is in cm below the sea floor. Lightly shaded zone indicates sapropel S1.

Figures 1 and 2 along with those elements that were recorded by the ITRAX instrument for the archive section of the core from which the data of Figures 1 and 2 were gathered (Table 1); and (ii) those elements recorded by the ITRAX instrument for the two sections of core SL104 containing sapropels (Fig. 3). The ITRAX response (scan integrals) to the concentration of an element in sediments varies greatly between different elements (Table 1), and some elements with both low mean concentrations and low mean scanner integrals (e.g. S, As) prove critical for interpretation of the localized elemental enrichments in the sapropel.

On the following reasoning, seven element integral ratios and one direct integral from the element scans were selected to identify critical sapropel features.

- *Ba/Ti integrals ratio*. High Ba/Al levels have been shown to occur in sapropels where C_{org} values are high, due to the presence of biogenic Ba associated with organic matter, and these high Ba/Al values appear to be preserved in sapropels even if C_{org} is oxidized at a later stage (Thomson *et al.* 1995, 1999; van Santvoort *et al.* 1996, 1997). Aluminium was not detected efficiently with the ITRAX configuration used, and in the absence of Al data the possible alternatives as the element for detrital aluminosilicate normalization among the elements detected by ITRAX (Table 1) are Ti, K and Rb. Although Lourens *et al.* (2001) have demonstrated that the Ti/Al ratio in Pliocene eastern Mediterranean sediment sections containing sapropels shows a remarkable cyclicity with lower values in sapropels compared with the enclosing marls, this effect does not appear so marked in more recent sapropels (Fig. 1). Ba/Ti ratios were therefore selected on the expectation that they would behave similarly to Ba/Al ratios.
- *Br/Cl integrals ratio*. Marked enrichments in Br content are found in sapropels (Ten Haven *et al.* 1987; Mercone *et al.* 2001) (Fig. 2), partly due to an enrichment of Br with C_{org}, and partly due to the higher porosity and, hence, higher sea-salt content in the pore waters of the sapropel compared with the enclosing marls. The latter factor also causes relatively high Cl contents in sapropels.

Table 1. *Mean response of the ITRAX system over core LC21 section 11 compared with mean WD-XRF concentrations determined in individual samples from the same core section. The ITRAX data are the means of 1590 element peak area integrals, each collected over a width of 200 μm for 40 s at a spacing of 0.5 mm over 81 cm, while the WD-XRF data are 23 analyses of 1 cm-thick samples. Note that the concentrations of redox-sensitive elements in particular are highly variable in this section (Figs 1 & 2)*

Element	ITRAX Mean integral	ITRAX SD on mean	ITRAX SD/mean%	WD-XRF Mean ($\mu g\,g^{-1}$)	WD-XRF SD on mean	WD-XRF SD/mean%
Fe	167 646	19 087	11	28 418	2498	9
Ca	96 203	13 549	14	171 414	8516	5
Sr	54 567	5648	10	750	68	9
Zr	28 732*	860*	3*	78	6	8
Br	3752	1317	35	104	33	32
Ni	3600	414	11	211	19	9
K	3472	812	23	2402	786	33
Rb	3171	482	15	n.a.†		
Co	3142	847	27	n.a.†		
Ti	2592	336	13	2285	135	6
Mn	2284	5243	230	1676	1668	99
Zn	1055	173	16	66	3	5
Cu	973	214	22	71	10	14
Cl	923	197	21	22 578	7280	32
Cr	622	213	34	197	10	5
As	483	543	112	10	12	117
V	127	113	89	128	46	36
Pb	122	87	71	12	2	14
Ba	95	63	67	316	135	43
S	24	64	264	4343	2313	53
Si	n.d.‡			132 028	7228	5
Al	n.d.‡			41 739	2321	6
Mg	n.d.‡			29 848	1265	4

* Prototype ITRAX Zr data compromised by a detector contamination.
n.a.†: not available.
n.d.‡: not detected by the ITRAX system with the Mo target X-ray tube used.

The Ba/Cl ratio is chosen to reveal the presence of additional Br associated with C_{org} in excess of the constant Br/Cl sea-salt ratio.

- *Mn/Ti integrals ratio.* High Mn/Al values in two separated peaks are commonly observed above the visual S1 unit, as a result of oxidation of Mn^{2+} in the sediment pore waters or sea water to MnO_x by increased bottom water O_2 levels that become available at the end of sapropel formation (Thomson *et al.* 1995, 1999; Calvert & Pedersen 1996; van Santvoort *et al.* 1996). This parameter is important in defining the extent of post-depositional oxidation of sapropel.
- *Cu/Ti integrals ratio.* This ratio was initially included because Cu, like several other chalcophile elements, generally shows an increase in sapropels (Fig. 2). The ratio also turned out to be a useful marker of post-depositional oxidation, as discussed below.
- *Fe/Ti integrals ratio.* Pyrite (FeS_2) forms in sapropels (Passier *et al.* 1996, 1999), and the enrichment of Fe content causes an increase in the Fe/Ti ratio over the assumed constant Fe/Ti detrital value.
- *S/Cl integrals ratio.* The S/Cl ratio is chosen to reveal the presence of additional S associated with pyrite or C_{org} (Passier *et al.* 1999) in excess of the constant S/Cl sea-salt ratio.
- *As integral.* Arsenic is strongly incorporated into FeS_2 (Peterson & Carpenter 1986; Huerta-Diaz & Morse 1992). Arsenic data have not been normalized to Ti because As is generally close to its XRF limit of detection except where pyrite occurs (cf. Fig. 2).
- *Sr/Ca integrals ratio.* This ratio is monitored because the Sr/Ca ratio in sapropel units has been reported to be consistently higher than in the enclosing marls (Calvert 1983). The substantial $CaCO_3$ content in eastern Mediterranean sediments (e.g. generally 40–50%, Fig. 1) means that an increased Sr/Ca ratio requires the presence of some phase with an unusually high Sr/Ca ratio. This has been identified as aragonite that has been postulated to form as a consequence

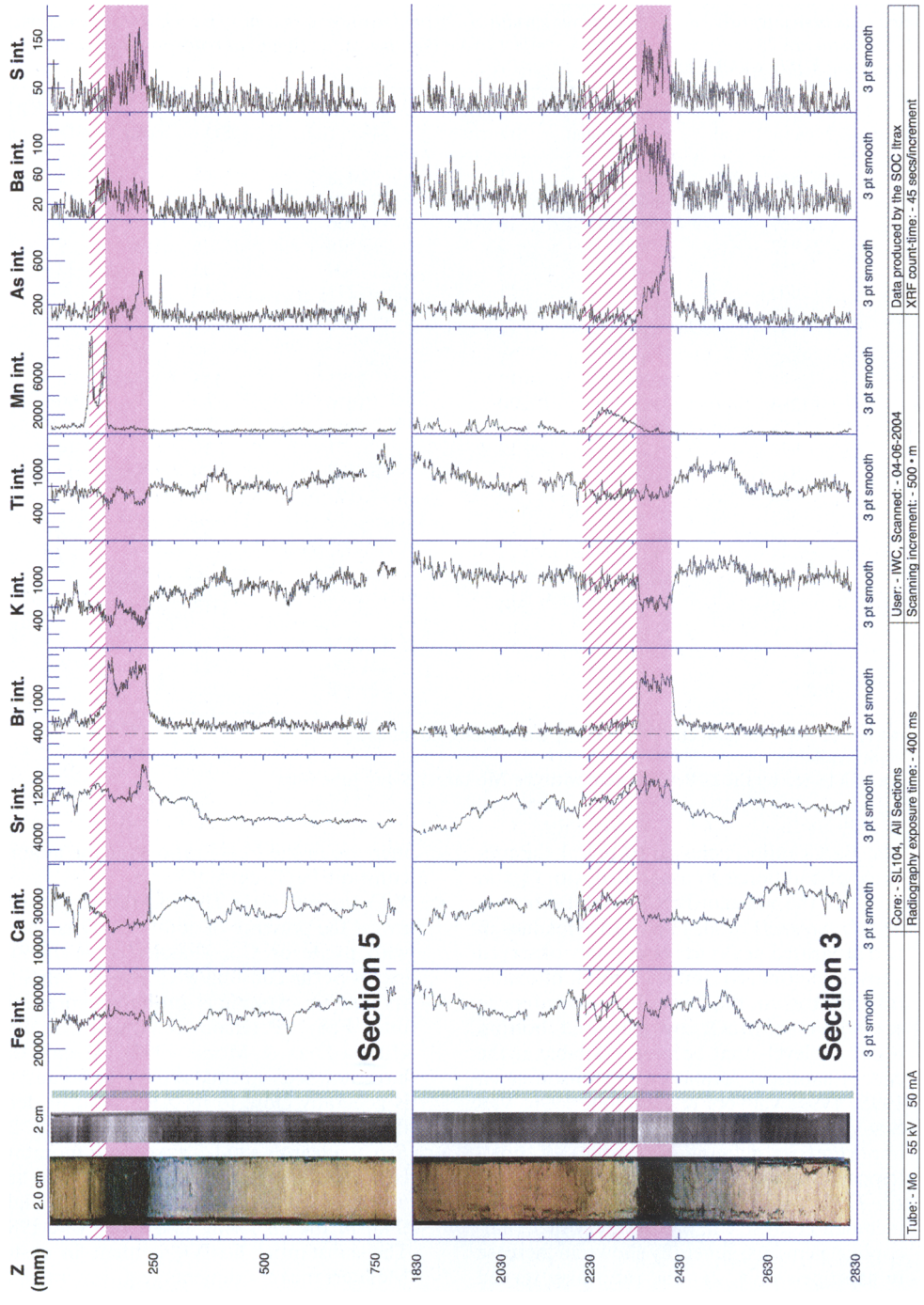

of the alkalinity produced by sulphate reduction diagenesis within sapropels (Thomson *et al.* 2004).

Inorganic geochemistry of sapropel S1 as revealed by ITRAX in section 5, core SL104

Sapropel S1 is present as a dark band at 130–230 mm in the uppermost section 5 of core SL104. When submitted to ITRAX analysis, the dark band in the visual image is revealed by the X-radiograph to have a lower sediment density than the remainder of the section (Figs 3 & 4). This lower density of the sapropel sediments is due to their increased porosity, as revealed by the increased Cl content from the increased pore-water content per unit sediment volume, and is the cause of increased Compton (incoherent) scattering in the sapropel (Fig. 4). This may be the reason for the local effect seen in the K/Ti ratio that was expected to be approximately constant from WD-XRF data on sapropel S1.

High values of the Ba/Ti and Br/Cl ratios are present through the 10 cm-thick dark band, but while the Br/Cl ratio is high in exact coincidence with the dark coloration, high values of the Ba/Ti ratio continue for approximately 4 cm immediately above it (90–130 mm; Fig. 4). The Ba/Ti ratio profile also has a central minimum, similar to the two peaks in the Ba/Al ratio that follow the fluctuation of C_{org} in the two sapropel lobes in core LC21 (Fig. 1). Two clear peaks in the Mn/Ti ratio occur immediately above the visual sapropel, the upper of which has its maximum coincident with the point where high Ba/Ti values return to the detrital baseline, while the lower has its maximum on the upper face of the visual sapropel where Br/Cl values return to the salt baseline (Fig. 4). Such Ba, Mn and Br profiles are interpreted as due to the oxidation of C_{org} and sulphide from the upper reaches of the original sapropel S1 by bottom-water O_2, with the upper Mn peak marking the end of sapropel formation and the lower Mn peak marking the progress of oxidation into the sapropel since that time (Thomson *et al.* 1995, 1999; van Santvoort *et al.* 1996). (Note that core LC21 (Figs 1 & 2) was selected for intensive study by Mercone *et al.* (2000, 2001) because the sediments of that core had accumulated so rapidly that these post-depositional oxidation effects on the S1 unit were minor or absent in that core.) The Br/Cl and Ba/Ti profiles in core SL104 section 5 are consistent with a loss of Br along with C_{org} on oxidation (Shimmield & Pedersen 1990), whereas Ba is retained after C_{org} oxidation (Thomson *et al.* 1995, 1999). In this example, the sapropel is interpreted as having been 14 cm thick initially, with the upper 4 cm oxidized since deposition and the lower 10 cm remaining as the present visual sapropel. As the top of the visual S1 unit is only 13 cm below the sea floor, this oxidation of the sapropel is expected to be active, and expected to continue either until the sapropel is fully oxidized or for as long as bottom-water O_2 can diffuse down to the upper face of the sapropel.

While the maximum of the lower Mn/Ti peak is located immediately above the visual sapropel, a clear peak in Cu/Ti occurs immediately below this Mn/Ti peak, exactly at the top of the visual sapropel (Fig. 4). In the raw data, high Mn values fall off at exactly the same level as the highest value on the upper face of the Cu peak rises to fall off over <1 cm (Fig. 5). Other trace elements (Se, Hg and Ag) not detected by the ITRAX have also been shown previously to have large narrow peaks exactly at the top of the visual sapropel, i.e. on the anoxic side of the limit of oxidation (Mercone *et al.* 1999; Crusius & Thomson 2003). Such peaks are produced by the repeated mobilization of elements present at enhanced concentration in the original sapropel by oxidation with bottom-water O_2 after sapropel formation, followed by their repeated immobilization by reduction in the anoxic conditions of the unoxidized sapropel. These peaks are expected to move downwards below the advancing oxidation front and continue to be augmented for as long as the oxidation front is active. The peak should remain in place in anoxic conditions as a relict marker of the oxidation process thereafter. This feature does not appear to have been reported previously in sapropel Cu profiles, probably because of the relatively small size of the Cu/Ti peak relative to the detrital background in the lower-resolution sampling undertaken for conventional analysis that is generally undertaken on sample increments no finer than 0.5–1 cm thick.

The two Fe/Ti peaks in the sapropel are probably related to the two Ba/Ti peaks that should mark increases in C_{org} content which drives sulphate reduction, although the corroborative S/Cl and As evidence for pyrite formation is

Fig. 3. Colour photograph, X-radiograph and intensity v. depth profiles for the 10 elements with the largest integrals reported by the ITRAX ED-XRF on scans along sections 5 and 3 of core SL104. The XRF data are displayed as three-point running means of 45 s XRF integrals and the depth scale is the depth in core in mm. Shaded and diagonal-hatched backgrounds indicate the zones of unoxidized (residual or visual) sapropel and the inferred oxidized sapropel, respectively.

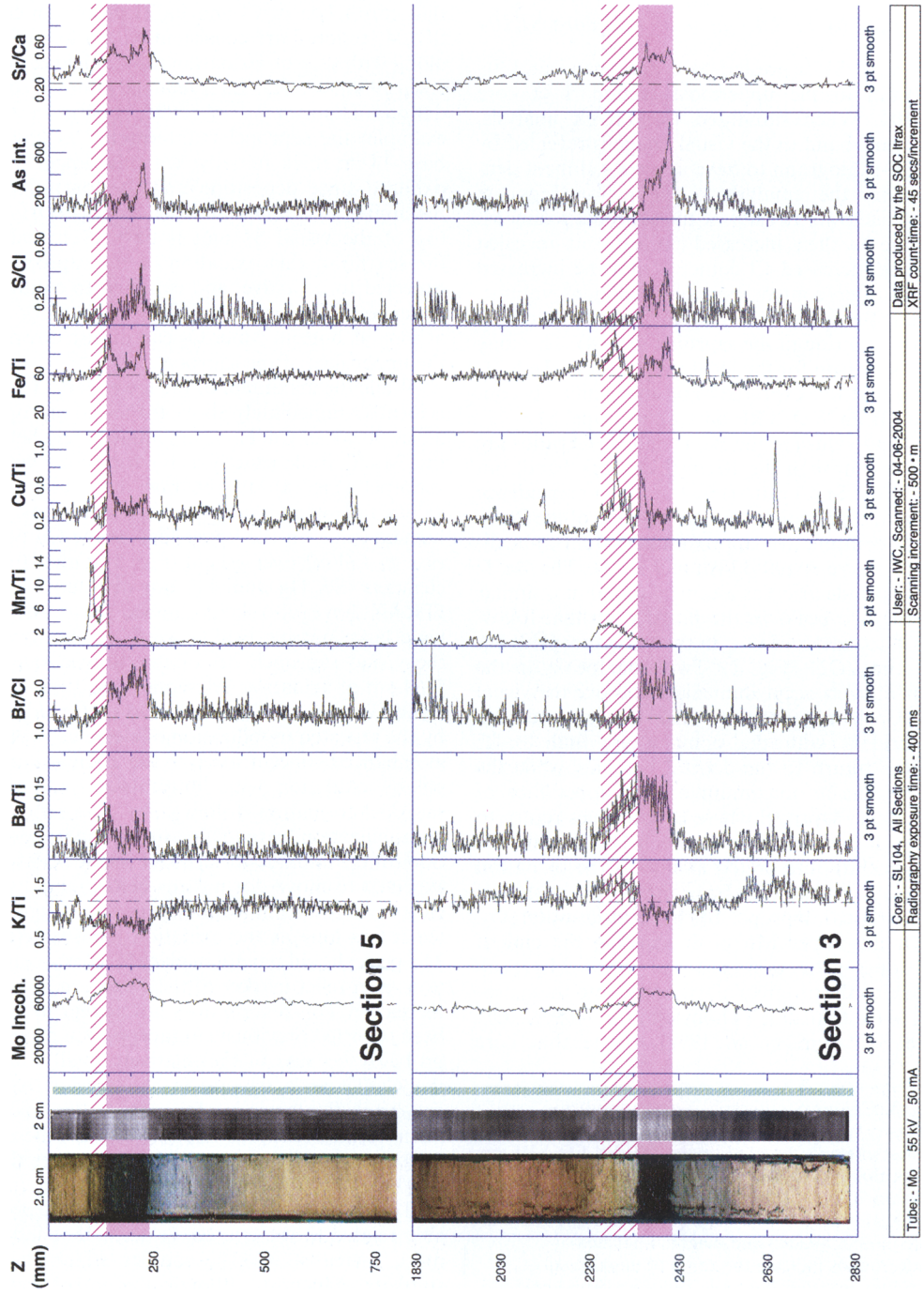

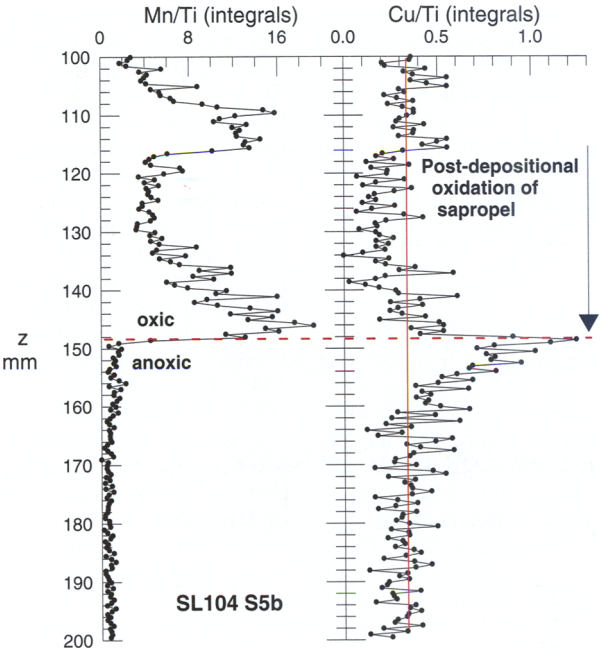

Fig. 5. Detail of the ITRAX Mn/Ti and Cu/Ti ED-XRF scans from section 5 of core SL104. These are the raw XRF count integral data plotted without smoothing. The level where Mn/Ti decreases and Cu/Ti increases (dotted line) marks the inferred location of the active oxidation front in this S1 sapropel.

now only present in the lower peak because of the effects of the inferred oxidation front (Fig. 4). The upper Fe peak with its maximum close to the upper face of the visual sapropel may have been initially present as FeS_2, as in the example of Figure 1. This peak must have formed later than the lower Fe/Ti peak, and it contains a much lower As concentration. The Fe/Ti, S/Cl and As profiles all suggest that pyritization has been most intense towards the base of the visual S1 unit. In a reverse of the explanation proposed above for the Cu/Ti peak at the limit of oxidation, the shapes of the Fe/Ti and As profiles, with maximum values at the lower face of the sapropel and peak shapes that tail upwards into the sapropel unit, probably indicate the direction of supply of the extra Fe and As now found in FeS_2. Berner (1969, 1984) has discussed how production of sulphide driven by organic matter oxidation with sulphate reacts with Fe^{2+} from the reduction of Fe oxyhydroxides in order to form diagenetic FeS_2. The situation in the S1 unit in core SL104 section 5 is similar to Berner's (1969) case where supply of Fe^{2+} is sufficient to consume the H_2S produced by sulphate reduction close to its locus of formation and thereby limit H_2S diffusion. Passier *et al.* (1996, 1999) have demonstrated that a diffusive export of sulphide out of sapropel units can occur, in which case FeS_2 forms below the sapropel, but in the case of the S1 unit in core SL104 the shapes of the Fe/Ti, S/Cl and As profiles suggest that most of the pyrite must have formed just inside the lower level of the sapropel. Consistent with this explanation, the lowest Fe/Ti values in this entire core section are found in the 20 cm-section immediately below the sapropel, which probably represents a loss of Fe oxyhydroxides that were reduced to Fe^{2+} that diffused upwards and is now immobilized in the sapropel as FeS_2. The colour of the sediment in this 20 cm-section has been altered from buff to grey, also suggesting localized reduction.

Fig. 4. Colour photograph, X-radiograph and ratios of the ITRAX ED-XRF scan integrals for the Mo Compton scatter peak, K/Ti, Ba/Ti, Br/Cl, Mn/Ti, Cu/Ti, Fe/Ti, S/Cl and Sr/Ca and the As integral as a function of depth in sections 5 and 3 of core SL104. The XRF data are displayed as three-point running means. The high water contents in the unoxidized S1 sapropel at 130–230 mm in section 5 and in the visual S3 unit in section 3 at 2350–2430 mm cause local increases in Compton (incoherent) scattering, and the resultant changes in excitation efficiency probably affect the expected constancy of the K/Ti ratio. Shaded and diagonal-hatched backgrounds indicate the zones of unoxidized (residual or visual) sapropel and the inferred oxidized sapropel, respectively.

The Sr/Ca profile (Fig. 4) has its maximum value close to the level of maximum pyrite formation. High Sr/Ca values in sapropels are indicative of the presence of aragonite (Thomson *et al.* 2004), and here these occur through both the residual and oxidized sections of the sapropel and for at least approximately 5 cm below. This is likely to reflect some diffusion of carbonate system species in solution before crystallization to aragonite.

Inorganic geochemistry of sapropel S3 as revealed by ITRAX in section 3, core SL104

Sapropel S2 is rarely reported in the eastern Mediterranean sedimentary record and its formation is controversial, but sapropel S3 did form approximately 85 ka ago (Bard *et al.* 2002). The S3 unit is clearly evident in both the visual image and the X-radiograph at 2350–2430 mm depth in core in section 3 of core SL104 (Figs 3 & 4). High Br/Cl values are exactly coincident with this 8 cm-thick lower-density dark band, but high Ba/Ti values continue through the dark band and for approximately 11 cm (2240–2350 mm) above it. By analogy with the Br/Cl and Ba/Ti profiles of sapropel S1 in this core discussed above, post-depositional oxidation of the upper 11 cm of an S3 sapropel that was originally 19 cm thick is indicated. In this case the overall Ba/Ti profile is Gaussian in shape without the central dip in the profile seen in the S1 sapropel (Figs 1 & 4), and the maximum Ba/Ti is up to 1.5 times that of the S1 sapropel (Fig. 4). Calvert & Fontugne (2001) have reported maximum C_{org} contents of 2.0 and 2.8 wt% C_{org} in sapropels S1 and S3, respectively, suggesting that the Ba/Ti ratio may be broadly proportional to C_{org} content in core SL104.

The sediments at the depths of section 3 in core SL104, almost 2 m below the sea floor, are now in anoxic conditions. The post-depositional oxidation of this S3 unit could only have continued for as long as diffusional contact with bottom-water O_2 was maintained, and all evidence of post-depositional oxidation of sapropel S3 must now be relict (van Santvoort *et al.* 1997). The Mn peaks at the tops of sapropels initially form as MnO_x containing Mn[IV] and Mn[III], which is unstable under anoxic conditions, so that any solid-phase Mn enrichment formed above sapropel S3 is expected to have been reduced on burial. It might therefore be expected that the Mn^{2+} produced by reduction would have diffused away in pore-water solution, but the largest solid-phase Mn/Ti peak in this core section still appears to be in position above the sapropel (Fig. 4). This Mn/Ti peak is broad and much smaller than the corresponding Mn/Ti peaks in sapropel S1, however, and lacks any evidence of the two sharp peaks that are characteristic of the active oxidation of sapropel S1 (e.g. Fig. 4). Another difference is that the excess Mn in the S3 unit appears to have penetrated slightly into the visible sapropel. One likely explanation is that diffusion of Mn^{2+} away from the site of MnO_x localization has been limited by sorption on to carbonate surfaces, a phenomenon that has been shown to be prevalent in carbonate-rich sediments (Boyle 1983; Thomson *et al.* 1986; Middelburg *et al.* 1987). A related possibility is the formation of a mixed Mn–Ca carbonate phase, a conversion process that forms authigenic carbonates as chemical laminations in the brackish sediments of Baltic Sea deeps after episodic oxygenation events (Huckriede & Meischner 1996). Kulik *et al.* (2000) have concluded that the critical requirement for Mn–Ca carbonate formation is the development of very high local pore-water Mn^{2+} concentrations from MnO_x reduction in the presence of alkalinity.

As in the S1 profile in section 5, there is a peak in the Cu/Ti profile with a flat upper face and a downwards tail over approximately 20 mm at the top of the visual sapropel at 2350 mm (Fig. 4). This peak shape and position is consistent with the inferred limit achieved by post-depositional oxidation in this sapropel when active. This is neither the largest nor the only Cu/Ti peak in this section, however. Two larger peaks, both with sharp upper cut-offs, are present at 2300 mm in the oxidized sapropel and at 2660 mm well below the sapropel. Localized enrichments with high Cu contents have been noted in deep-sea sediments elsewhere, although the mechanism for their formation and the source of the additional Cu remain enigmatic (Siesser 1976; van Os *et al.* 1993; Thomson *et al.* 1996). van Os *et al.* (1993) reported two different types of Cu enrichment, one that occurs in an association with other trace elements that appears similar to a MnO_x association, and a second that occurs as thin purple-coloured bands that fade rapidly with time (oxidize?) and are apparently associated only with S. Such purple bands do not appear to have been reported hitherto from sapropels, but van Os *et al.* (1993) have suggested that they result from mobilization of an unidentified Cu–S species from organic-rich turbidite units. Another possibility is that Cu is mobile in an organo-S complex rather than as a Cu–S species (e.g. Skrabal *et al.* 2000).

Pyritization of the S3 unit is revealed by the Fe/Ti and S/Cl ratios and As values. Again, pyrite formation is most intense just above the base of the sapropel, and the mean value of the Fe/Ti ratio is again lower for tens of cm below the sapropel than above it, consistent with a loss of Fe from reduction of oxyhydroxides to supply the extra Fe found in the sapropel as FeS_2 (Fig. 4). The cause of the second Fe peak in the oxidized section of sapropel S3 at 2310 mm is not clear. This peak is not associated with S or As, and it may represent solid-phase Fe(III) formed by a reduction and displacement of Mn(II) from $Mn(III,IV)O_x$ by Fe^{2+}, a process discussed by Postma & Appelo (2000).

The Sr/Ca profile in this section (Fig. 4) has its maximum in the visual sapropel but higher Sr/Ca values also occur approximately 30 cm above and about 20 cm below, much more widely spread than the corresponding Sr/Ca peak in S1. It is not clear whether this represents the initial pattern of formation of aragonite in and around this sapropel, or whether some later dissolution of aragonite with an outwards diffusion of Sr^{2+} has occurred.

Conclusions

Several similar geochemical characteristics could be recognized in the most recent sapropel S1 and in the older sapropel S3 through the combination of visual and X-radiograph images and XRF elemental ratio profiles obtained using the ITRAX core scanner. Element/Ti ratios of the semi-quantitative XRF integrals from the scanner appear to provide an acceptable alternative to the element/Al ratios that are customarily used to define detrital aluminosilicate levels, and element/Cl ratios can be employed to indicate where S and Br increase markedly over their seasalt values due to pyrite formation or association with C_{org}, respectively. Evidence of the localized enrichments of redox-sensitive elements associated with C_{org} or sulphide formation is readily identified in sapropels through the selected ratios, and profile trends reveal evidence of the oxidation that many sapropels undergo after deposition. The directions of movement of certain elements (Fe and As, Cu) during diagenesis can be inferred from profile shapes. The extra level of detail recorded by continuous high-resolution sampling with the finely collimated X-ray beam of the ITRAX provides a considerable advantage over conventional sampling and analysis, particularly for identification of narrow zones of unusually high concentrations of particular elements, such as the Cu localizations encountered in this study.

Data for this study were gathered with the prototype ITRAX system, but modifications and improvements to the primary X-ray excitation, X-ray detection and data processing of later ITRAX systems allow collection of quantitative data for a range of elements from Al through to Zr (Croudace *et al.* 2006). Such data are achievable on favourable fine-grained sample types (e.g. compressed rock powder), but calibrated data for a larger set of elements can now also be obtained from split cores. We make the caveat that such data should not be expected to be truly quantitative in all cases, however. On unprocessed sediment in cores, XRF scanner systems cannot be expected to deliver a quality of data comparable to that of WD-XRF systems because of the small excitation volume used, the air path, and the effects of mineralogical, particle size, porosity and water content variations. The primary strength of scanner systems is their analytical rapidity and the potential of their high-resolution capability to provide insights not possible with conventional methods where cm-scale discrete samples are required to provide sufficient material for analysis.

We gratefully acknowledge Professor C. Hemleben (Tübingen University, Chief Scientist of *Meteor* cruise 51-3), Professor E. Rohling (NOCS) and BOSCORF for access to the core sections used in this study, Ms K. Davis (NOCS) for assistance with the illustrations, and Professor Steve Calvert (University of British Columbia) for referee comments on the original manuscript.

References

BARD, E., DELAYGUE, G., ROSTEK, F., ANTONIOLI, F., SILENZI, S. & SCHRAG, D.P. 2002. Hydrological conditions over the western Mediterranean basin during the deposition of the cold Sapropel 6 (ca. 175 kyr BP). *Earth and Planetary Science Letters*, **202**, 481–494.

BERNER, R.A. 1969. Migration of iron and sulfur within anaerobic sediments during early diagenesis. *American Journal of Science*, **267**, 19–42.

BERNER, R.A. 1984. Sedimentary pyrite formation – An update. *Geochimica et Cosmochimica Acta*, **48**, 605–615.

BOYLE, E.A. 1983. Manganese carbonate overgrowths on foraminifera tests. *Geochimica et Cosmochimica Acta*, **47**, 1815–1819.

CALVERT, S.E. 1983. Geochemistry of Pleistocene sapropels and associated sediments from the eastern Mediterranean. *Oceanologica Acta*, **6**, 255–267.

CALVERT, S.E. & FONTUGNE, M.R. 2001. On the late Pleistocene–Holocene sapropel record of climatic and oceanographic variability in the eastern Mediterranean. *Paleoceanography*, **16**, 78–94.

CALVERT, S.E. & PEDERSEN, T.F. 1996. Sedimentary geochemistry of manganese: Implications for the

environment of formation of manganiferous black shales. *Economic Geology*, **91**, 36–47.

CASFORD, J.S.L., ABU-ZIED, R. *ET AL.* 2001. Mediterranean climate variability during the Holocene. *Mediterranean Marine Science*, **2**, 45–55.

CASFORD, J.S.L., ROHLING, E.J. *ET AL.* 2003. A dynamic concept for eastern Mediterranean circulation and oxygenation during sapropel formation. *Palaeogeography, Palaeoclimatology, Palaeoecology*, **190**, 103–119.

CROUDACE, I.W., RINDBY, A. & ROTHWELL, R.G. 2006. ITRAX: Description and evaluation of a new multi-function X-ray core scanner. *In*: ROTHWELL, R.G. (ed.) *New Techniques in Sediment Core Analysis*. Geological Society, London, Special Publications, **267**, 51–63.

CRUSIUS, J. & THOMSON, J. 2003. Mobility of authigenic rhenium, silver and selenium during post-depositional oxidation in marine sediments. *Geochimica et Cosmochimica Acta*, **67**, 265–273.

HEBBELN, D. & CORTES, J. 2001. Sedimentation in a tropical fjord: Golfo Dulce, Costa Rica. *Geo-Marine Letters*, **20**, 142–148.

HEMLEBEN, C., HOERNLE, K., JORGENSON, B.B. & ROETHER, W. (eds). 2001. *Ostatlantic – Mittelmeer – Schwarzes Meer, Cruise No. 51, 12 September–28 December 2001*. METEOR Berichte, Universitat Hamburg, **03-1**.

HILGEN, F.J. 1991. Astronomical calibration of Gauss to Matuyama sapropels in the Mediterranean and implication for the geomagnetic polarity time scale. *Earth and Planetary Science Letters*, **104**, 226–244.

HUCKRIEDE, H. & MEISCHNER, D. 1996. Origin and environment of manganese-rich sediments within black-shale basins. *Geochimica et Cosmochimica Acta*, **60**, 1399–1413.

HUERTA-DIAZ, M.A. & MORSE, J.W. 1992. Pyritisation of trace metals in anoxic marine sediments. *Geochimica et Cosmochimica Acta*, **56**, 2681–2702.

JANSEN, J.H.F., VAN DER GAAST, S.J., KOSTER, B. & VAARS, A.J. 1998. CORTEX, a shipboard XRF-scanner for element analyses in split sediment cores. *Marine Geology*, **151**, 143–153.

KULIK, D.A., KERSTEN, M., HEISER, U. & NEUMANN, T. 2000. Application of Gibbs Energy minimization to model early-diagenetic solid-solution aqueous-solution equilibria involving authigenic rhodochrosites in anoxic Baltic Sea sediments. *Aquatic Geochemistry*, **6**, 147–199.

LOURENS, L.J., ANTONARAKOU, A., HILGEN, F.J., VAN HOOF, A.A.M., VERGNAUD-GRAZZINI, C. & ZACHARIASSE, W.J. 1996. Evaluation of the Plio-Pleistocene astronomical timescale. *Paleoceanography*, **11**, 391–413.

LOURENS, L.J., WEHAUSEN, R. & BRUMSACK, H.J. 2001. Geological constraints on tidal dissipation and dynamical ellipticity of the Earth over the past three million years. *Nature*, **409**, 1029–1033.

MERCONE, D., THOMSON, J., ABU-ZIED, R.H., CROUDACE, I.W. & ROHLING, E.J. 2001. High-resolution geochemical and micropalaeontological profiling of the most recent eastern Mediterranean sapropel. *Marine Geology*, **177**, 25–44.

MERCONE, D., THOMSON, J., CROUDACE, I.W., SIANI, G., PATERNE, M. & TROELSTRA, S. 2000. Duration of S1, the most recent sapropel in the eastern Mediterranean Sea, as indicated by AMS radiocarbon and geochemical evidence. *Paleoceanography*, **15**, 336–347.

MERCONE, D., THOMSON, J., CROUDACE, I.W. & TROELSTRA, S.R. 1999. A coupled natural immobilisation mechanism for mercury and selenium in deep-sea sediments. *Geochimica et Cosmochimica Acta*, **63**, 1481–1488.

MIDDELBURG, J.J., DE LANGE, G.J. & VAN DER WEIJDEN, C.H. 1987. Manganese solubility control in marine pore waters. *Geochimica et Cosmochimica Acta*, **51**, 759–763.

NIJENHUIS, I.A., BOSCH, H.-J., SINNINGHE DAMSTÉ, J.S., BRUMSACK, H.-J. & DE LANGE, G.J. 1999. Organic matter and trace element rich sapropels and black shales: a geochemical comparison. *Earth and Planetary Science Letters*, **169**, 277–290.

PALIKE, H., SHACKLETON, N.J. & ROHL, U. 2001. Astronomical forcing in Late Eocene marine sediments. *Earth and Planetary Science Letters*, **193**, 589–602.

PASSIER, H.F., MIDDELBURG, J.J., DE LANGE, G.J. & BOTTCHER, M.E. 1999. Modes of sapropel formation in the eastern Mediterranean: some constraints based on pyrite properties. *Marine Geology*, **153**, 199–219.

PASSIER, H.F., MIDDELBURG, J.J., VAN OS, B.J.H. & DE LANGE, G.J. 1996. Diagenetic pyritisation under eastern Mediterranean sapropels caused by downward sulphide diffusion. *Geochimica et Cosmochimica Acta*, **60**, 751–763.

PETERSON, M.L. & CARPENTER, R. 1986. Arsenic distributions in pore waters and sediments of Puget Sound, Lake Washington, the Washington coast and Saanich Inlet, BC. *Geochimica et Cosmochimica Acta*, **50**, 353–369.

PETERSON, L.C., HAUG, G.H., HUGHEN, K.A. & ROHL, U. 2000. Rapid changes in the hydrologic cycle of the tropical Atlantic during the last glacial. *Science*, **290**, 1947–1951.

POSTMA, D. & APPELO, C.A.J. 2000. Reduction of Mn-oxides by ferrous iron in a flow system: Column experiment and reactive transport modeling. *Geochimica et Cosmochimica Acta*, **64**, 1237–1247.

RICHTER, T.O., LASSEN, S., VAN WEERING, T.C.E. & DE HAAS, H. 2001. Magnetic susceptibility patterns and provenance of ice-rafted material at Feni Drift, Rockall Trough: implications for the history of the British-Irish ice sheet. *Marine Geology*, **173**, 37–54.

ROHLING, E.J., MAYEWSKI, P.A., ABU-ZIED, R.H., CASFORD, J.S.L. & HAYES, A. 2002. Holocene atmosphere–ocean interactions: records from Greenland and the Aegean Sea. *Climate Dynamics*, **18**, 587–593.

ROLLINSON, H.R. 1993. *Using Geochemical Data: Evaluation, Presentation, Interpretation*. Pearson, Harlow, Longman NJ.

ROSSIGNOL-STRICK, M. 1983. African monsoons, an immediate climate response to orbital insolation. *Nature*, **304**, 46–49.

ROTHWELL, R.G. 1995. *Cruise Report*: Marion Dufresne *Cruise 81. Mediterranean Giant Piston Coring Transect*. NOL, Southampton. Unpublished report.

ROTHWELL, R.G., HOOGAKKER, B., THOMSON, J., CROUDACE, I.W. & FRENZ, M. 2006. Turbidite emplacement on the southern Balearic Abyssal Plain (western Mediterranean Sea) during Marine Isotope Stages 1–3: an application of ITRAX XRF scanning of sediment cores to lithostratigraphic analysis. *In*: ROTHWELL, R.G. (ed.) *New Techniques in Sediment Core Analysis*. Geological Society, London, Special Publications, **267**, 79–98.

SHIMMIELD, G.B. & PEDERSEN, T.F. 1990. The geochemistry of reactive trace metals and halogens in hemipelagic continental margin sediments. *Reviews in Aquatic Science*, **3**, 255–279.

SIESSER, W.G. 1976. Native copper in DSDP sediment cores from the Angola Basin. *Nature*, **263**, 308–309.

SKRABAL, S.A., DONAT, J.R. & BURDIGE, D.J. 2000. Pore water distributions of dissolved copper and copper-complexing ligands in estuarine and coastal marine sediments. *Geochimica et Cosmochimica Acta*, **64**, 1843–1857.

TEN HAVEN, H.L., DE LEEUW, J.W., SCHENK, P.A. & KLAVER, G.T. 1987. Geochemistry of Mediterranean sediments. Bromine/organic carbon and uranium/organic carbon ratios as indicators for different sources of input and post-depositional oxidation, respectively. *Organic Geochemistry*, **13**, 255–261.

THOMSON, J., CRUDELI, D., DE LANGE, G.J., SLOMP, C.P., ERBA, E., CORSELLI, C. & CALVERT, S.E. 2004. *Florisphaera profunda* and the origin and diagenesis of carbonate phases in eastern Mediterranean sapropel units. *Paleoceanography*, **19**, 1–19. PA3003 doi:10.1029/2003PA000976.

THOMSON, J., HIGGS, N.C. & COLLEY, S. 1996. Diagenetic redistributions of redox-sensitive elements in northeast Atlantic glacial/interglacial transition sediments. *Earth and Planetary Science Letters*, **139**, 365–377.

THOMSON, J., HIGGS, N.C., JARVIS, I., HYDES, D.J., COLLEY S. & WILSON, T.R.S. 1986. The behaviour of manganese in Atlantic carbonate sediments. *Geochimica et Cosmochimica Acta*, **50**, 1807–1818.

THOMSON, J., HIGGS, N.C., WILSON, T.R.S., CROUDACE, I.W., DE LANGE, G.J. & VAN SANTVOORT, P.J.M. 1995. Redistribution and geochemical behaviour of redox-sensitive elements around S1, the most recent Eastern Mediterranean sapropel. *Geochimica et Cosmochimica Acta*, **59**, 3487–3501.

THOMSON, J., MERCONE, D., DE LANGE, G.J. & VAN SANTVOORT, P.J.M. 1999. Review of recent advances in the interpretation of eastern Mediterranean sapropel S1 from geochemical evidence. *Marine Geology*, **153**, 77–89.

TUENTER, E., WEBER, S.L., HILGEN, F.J. & LOURENS L.J. 2003. The response of the African summer monsoon to remote and local forcing due to precession and obliquity. *Global and Planetary Change*, **36**, 219–235.

VAN DER WEIJDEN, C.H. 2002. Pitfalls of normalization of marine geochemical data using a common divisor. *Marine Geology*, **184**, 167–187.

VAN OS, B., VISSER, H.J., MIDDELBURG, J.J. & DE LANGE, G.J. 1993. Occurrence of thin, metal-rich layers in deep-sea sediments – A geochemical characterization of copper. *Deep-Sea Research, I*, **40**, 1713–1730.

VAN SANTVOORT, P.J.M., DE LANGE, G.J., LANGEREIS, C.G., DEKKERS, M.J. & PATERNE, M. 1997. Geochemical and paleomagnetic evidence for the occurrence of 'missing' sapropels in eastern Mediterranean sediments. *Paleoceanography*, **12**, 773–786.

VAN SANTVOORT, P.J.M., DE LANGE, G.J., THOMSON, J., CUSSEN, H., WILSON, T.R.S., KROM, M.D. & STROHLE, K. 1996. Active post-depositional oxidation of the most recent sapropel (S1) in sediments of the eastern Mediterranean Sea. *Geochimica et Cosmochimica Acta*, **60**, 4007–4024.

WEEKS, R., LAJ, C. *ET AL.* 1993. Improvements in long-core measurement techniques: applications in palaeomagnetism and palaeoceanography. *Geophysical Journal International*, **114**, 651–662.

WEHAUSEN, R. & BRUMSACK, H.J. 2000. Chemical cycles in Pliocene sapropel-bearing and sapropel-barren eastern Mediterranean sediments. *Palaeogeography, Palaeoclimatology, Palaeoecology*, **158**, 325–352.